Ghosts in ISOCAM images

K. Okumura[1], M. Pérault[1,2], Y. Longval[1]

November 4, 1998

1 : IAS, Université Paris XI, Bât.121, 91405 Orsay Cedex, France
2 : ENS Radioastronomie, 24 rue Lhomond, 75231 Paris Cedex 05, France

version : 1.1

1 Introduction

The problem of undesirable light due to the reflection on the detector surface was clearly raised by Aerospatiale in the design phase of ISOCAM, but was then overlooked. It was raised again during the pre-flight tests of the camera, which prompted to a few minor adjustments: filter tilting, aperture stop re-sizing, field mirror re-sizing, which improved the situation but did not completely eliminate the nuisance (Pérault et al. 1994 [6]). The major problem caused by the multiple reflection is seen as ghost images through 3, 6 and 12 arcsec pixel-field-of-view (PFOV) lenses. This ghost image is formed on the detector after two reflections: on the detector and on the filter. The ISOCAM's filters have then been tilted by 5° in order to avoid multiple reflections toward the detector. For this purpose, the filter mounts have been redesigned to meet the requirement. However, the circular variable filters (CVFs) are extended over a quarter of the circumference of the filter wheel and the tilting solution was not possible to adopt only by redesigning their mounts. Therefore the CVFs have been left without any modification and the problem of multiple reflection revealed in the ground tests remained in the in-flight data.

All the ISOCAM observations performed with CVFs are affected by this undesirable light and, as it is shown below, even some ISOCAM observations with a filter may also be affected (a tilt of 5° is not enough for some configurations). Therefore the observers should be aware of this alteration of their data. The following summarizes our present knowledge of the ghost in ISOCAM images, and its relation to flat-field distortion.

2 Observed ghost images with ISOCAM

Some calibration observations have been dedicated to the measurements of the undesirable light. Tab. 1 and Tab. 2 list these dedicated observations. We describe the ghosts in this report, but the influence of a strong source from outside the ISOCAM field-of-view is also very important to be warned. The stray light measurement performed with NML Cygnus in Rev. 46 shows an interesting result. Fig. 1 shows the raster scans used around the source. The Z-axis of the spacecraft was at 209° from the North projected on the sky. The orientations of the 6 rasters had been chosen so as to keep the bright source out of the other instruments' aperture. The raster step was 3 arcmin and the closest raster point from the source was at 4.6 arcmin. Also shown are the sequence numbers of the rasters beside the first raster point. This strong source at 4.6 arcmin from the ISOCAM field center gives rise to a stray light in a straight line pattern

Table 1: **Stray-light related calibration observations**

Filter	Lens	TDT No.	Target	Gain	Tint	Mirror	Raster	Comments
LW7	6.0"	01401010	HIC74083	1	2.10	l	staring	Point source
LW7	Pupil	01401111	HIC74083	2	2.10	l	staring	Pupil image
LW7	Pupil	01401212	HIC74083-off	2	2.10	l	staring	Blurred pupil image
LW7	6.0"	01401313	HIC74083-off	2	2.10	l	staring	Extended source
SW5	6.0"	01401716	HIC73005	1	2.10	s	staring	Point source
SW5	Pupil	01401817	HIC73005	2	2.10	s	staring	Pupil image
LW3	Pupil	02202109	HIC102422	2	2.10	l	3×3	Pupil image
LW3	Pupil	02202210	HIC64394	2	2.10	l	3×3	Pupil image
LW10	Pupil	03004502	HIC102422-off	2	2.10	l	staring	Blurred pupil image
LW10	Pupil	03004603	HIC102422	2	0.28	l	staring	Pupil image
LW4	6.0"	04606402-06907	NML Cygnus	2	2.10	l	6 5×1	straylight
SW5	Pupil	06602406	HIC64394-off	2	2.10	l	staring	Blurred pupil image
SW5	Pupil	06602507	HIC64394	2	0.28	l	staring	Pupil images

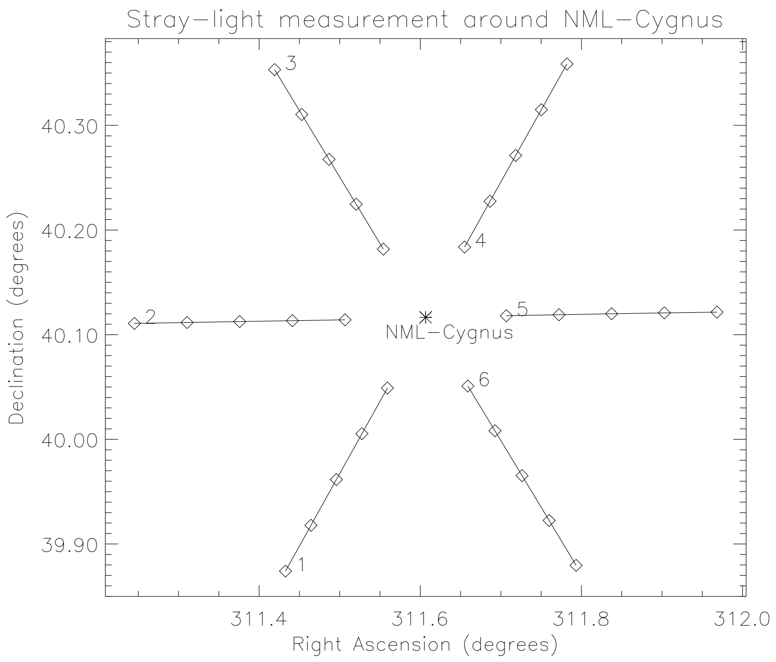

Figure 1: **Raster scans used for the stray-light measurement in Rev.46**

Table 2: ghost related calibration observations

Filter	Lens	TDT No.	Target	Gain	Tint	Mirror	Raster	Comments
LW1	3.0"	73000804	HIC98962	1	0.28	l	9×9	
LW1	6.0"	73001003	HIC96441	1	0.28	l	9×9	
LW1	6.0"	82501502	HIC94890	1	0.28	l	9×9	
LW2	1.5"	80102303	HIC99663	1	0.28	s	5×5	
LW2	3.0"	65500601	HIC77760	1	0.28	l	9×9	
LW2	6.0"	62600201	HIC77760	1	0.28	l	9×9	
LW3	1.5"	80102201	HIC98073	1	2.10	s	5×5	
LW3	3.0"	62600502	HIC80331	1	0.28	l	9×9	
LW3	6.0"	57600701	HIC87585	1	0.28	l	9×9	
LW3	6.0"	65500201	HIC80331	1	0.28	l	staring	lens jitter influence
LW3	6.0"	74004802	HIC87585	1	0.28	l	7×10	discontinuity
LW7	3.0"	74101706	HIC102422	1	0.28	l	9×9	
LW7	6.0"	73000905	HIC92782	1	0.28	l	9×9	
LW8	3.0"	65500204	HIC80331	1	0.28	l	staring	field mirror influence
LW8	6.0"	65500203	HIC80331	1	0.28	l	staring	lens jitter influence
LW10	3.0"	73000902	HIC92782	1	0.28	l	9×9	
LW10	6.0"	73000801	HIC98962	1	0.28	l	9×9	
CVF1 5μm	1.5"	62600101	Gamma Dra	1	0.28	s	5×5	pointing pb
CVF1 5μm	3.0"	57600801	Delta Dra	1	2.10	l	6×4	
CVF1 5μm	3.0"	73000701	Delta Dra	2	2.10	s	6×4	
CVF1 5μm	3.0"	84602202	Delta Dra	1	2.10	s	staring	lens jitter again
CVF1 5μm	6.0"	53101501	Delta Dra	2	0.28	l	9×5	
CVF1 5μm	6.0"	74005002	Delta Dra	1	0.28	l	8×16	discontinuity
CVF1 5μm	6.0"	84602303	Delta Dra	1	2.10	s	staring	lens jitter again
CVF1 7μm	1.5"	62600101	Gamma Dra	1	0.28	s	5×5	pointing pb
CVF1 7μm	3.0"	73000701	Delta Dra	2	2.10	s	6×4	
CVF1 7μm	3.0"	57600802	Delta Dra	1	2.10	l	6×4	
CVF1 7μm	6.0"	53101602	Delta Dra	2	0.28	l	9×5	
CVF1 9μm	1.5"	62600101	Gamma Dra	1	0.28	s	5×5	pointing pb
CVF1 9μm	3.0"	57600803	Delta Dra	1	2.10	l	6×4	
CVF1 9μm	3.0"	73000701	Delta Dra	2	2.10	s	6×4	
CVF1 9μm	6.0"	53800403	Delta Dra	2	0.28	l	9×5	
CVF1 9μm	6.0"	74005003	Delta Dra	1	0.28	l	8×16	discontinuity
CVF2 9μm	1.5"	62600101	Gamma Dra	1	0.28	s	5×5	pointing pb
CVF2 9μm	1.5"	77001002	Gamma Dra	1	0.28	s	5×5	
CVF2 9μm	3.0"	57600804	Delta Dra	1	2.10	l	6×4	
CVF2 9μm	3.0"	77001205	Delta Dra	2	0.28	s	6×4	not enough S/N
CVF2 9μm	3.0"	85300202	Delta Dra	1	2.10	s	6×4	better S/N
CVF2 9μm	6.0"	53800504	Delta Dra	2	0.28	l	9×5	
CVF2 12μm	1.5"	62600101	Gamma Dra	1	0.28	s	5×5	pointing pb
CVF2 12μm	1.5"	77001002	Gamma Dra	1	0.28	s	5×5	
CVF2 12μm	3.0"	57600805	Delta Dra	1	2.10	l	6×4	
CVF2 12μm	3.0"	77001205	Delta Dra	2	0.28	s	6×4	not enough S/N
CVF2 12μm	3.0"	85300202	Delta Dra	1	2.10	s	6×4	better S/N
CVF2 12μm	6.0"	53201005	Delta Dra	2	0.28	l	9×5	
CVF2 15μm	1.5"	62600101	Gamma Dra	1	0.28	s	5×5	pointing pb
CVF2 15μm	1.5"	77001002	Gamma Dra	1	0.28	s	5×5	
CVF2 15μm	3.0"	57600806	Delta Dra	1	2.10	l	6×4	
CVF2 15μm	3.0"	77001205	Delta Dra	2	0.28	s	6×4	not enough S/N
CVF2 15μm	3.0"	85300202	Delta Dra	1	2.10	s	6×4	better S/N
CVF2 15μm	6.0"	57600420	Delta Dra	2	0.28	l	9×5	

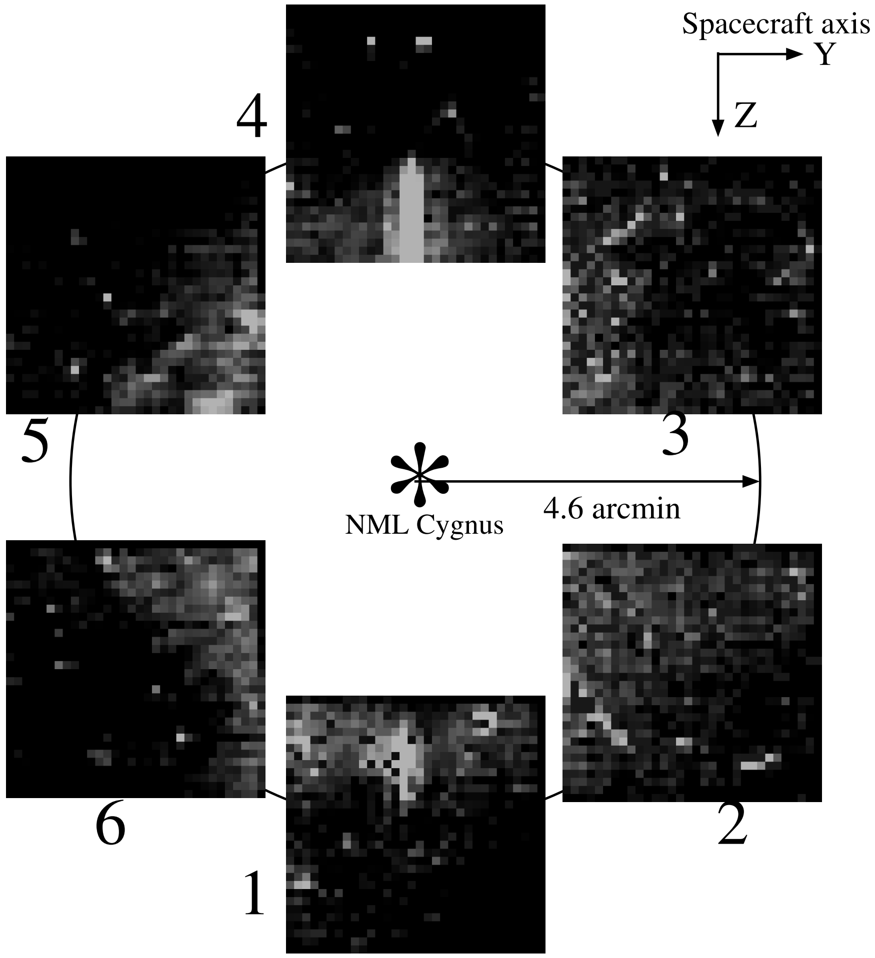

Figure 2: Stray-light measurement with NML Cygnus

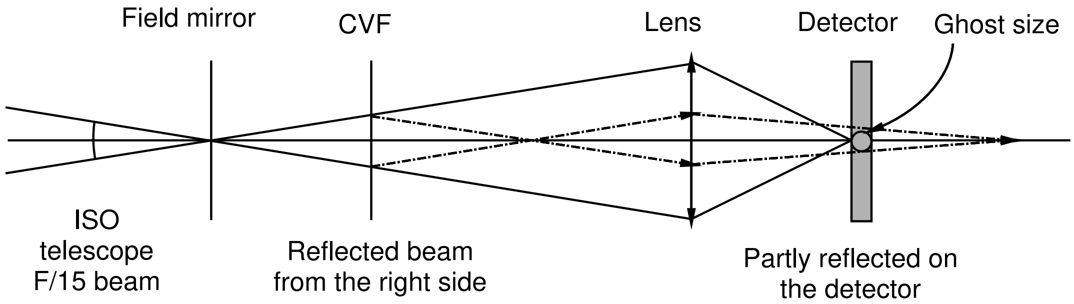

Figure 3: Optical path of the primary ghost in ISOCAM

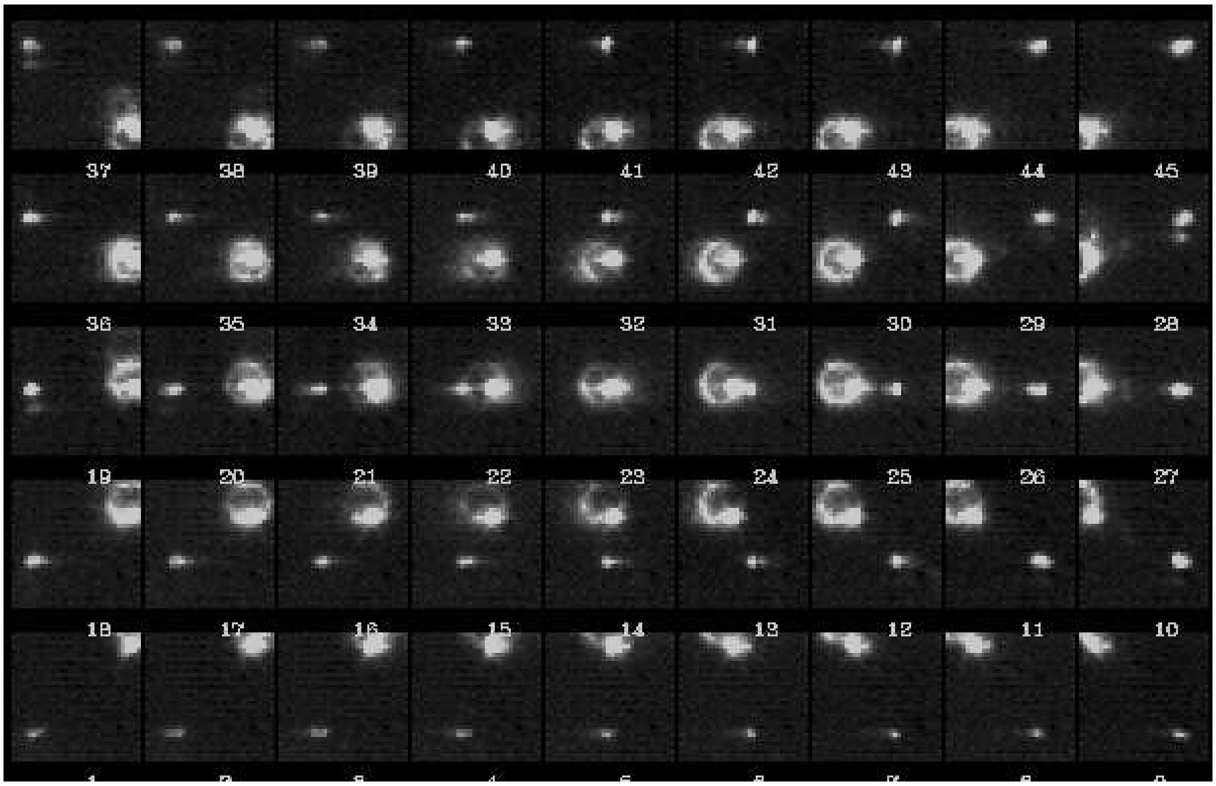

Figure 4: Global behaviour of ghosts when a point source moves over the detector (CVF at 7 μm with 6 arcsec PFOV in Rev. 531)

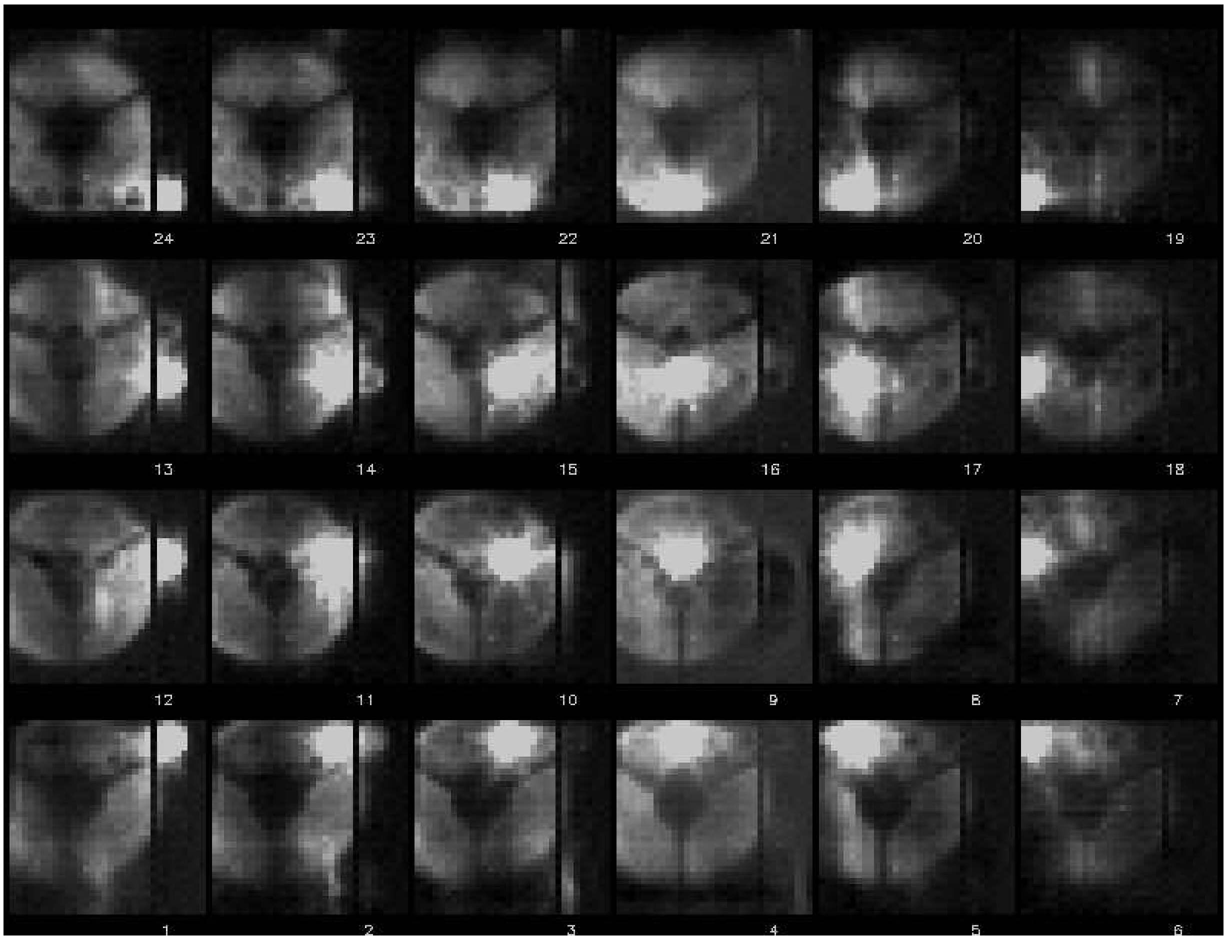

Figure 5: Global behaviour of ghosts when a point source moves over the detector (CVF at 5 μm with 3 arcsec PFOV in Rev. 730)

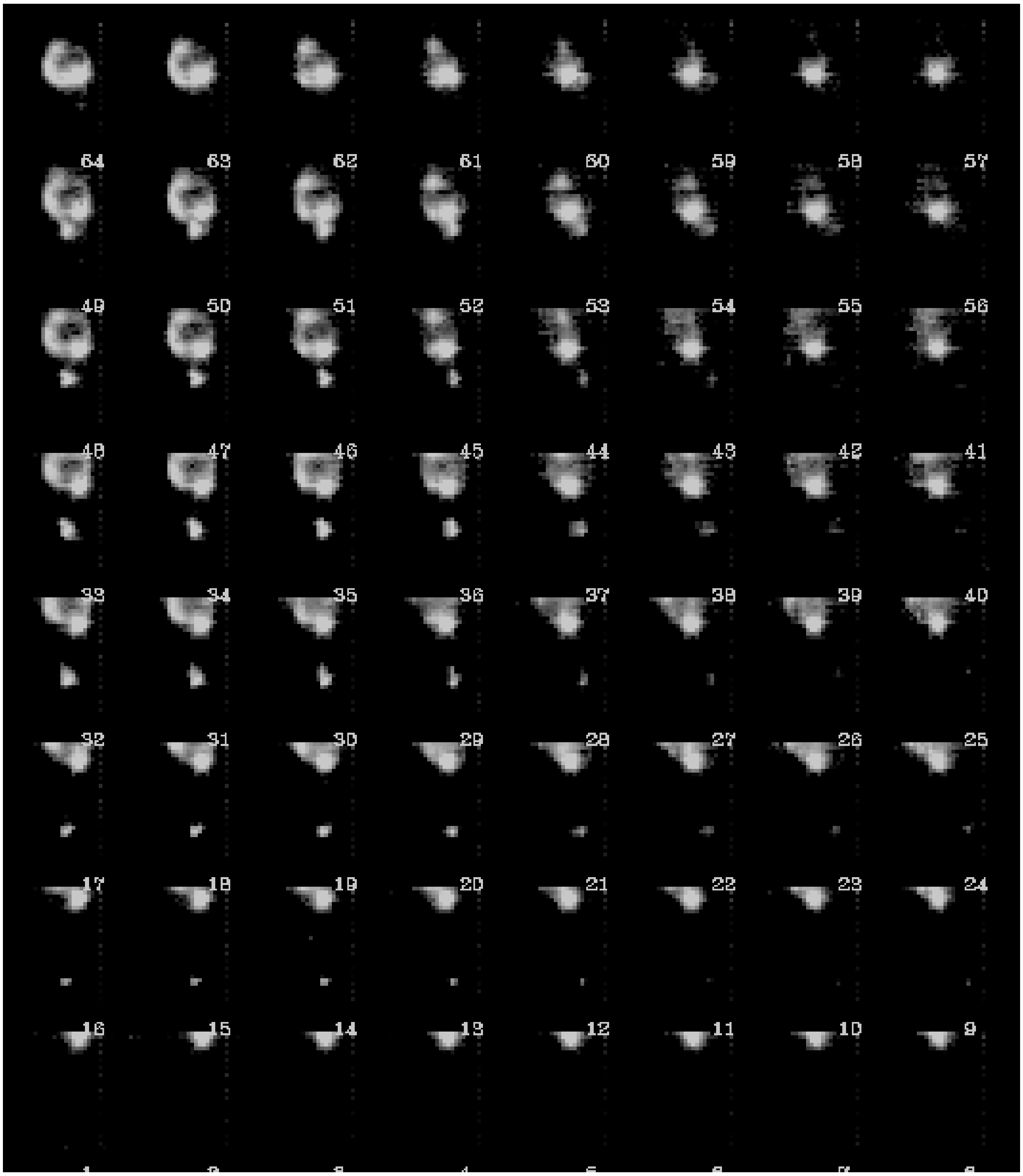

Figure 6: Discontinuous behaviour of ghosts when a point source moves around this region of the first half of a 8×16 raster (CVF at 5 μm with 6 arcsec PFOV in Rev. 740)

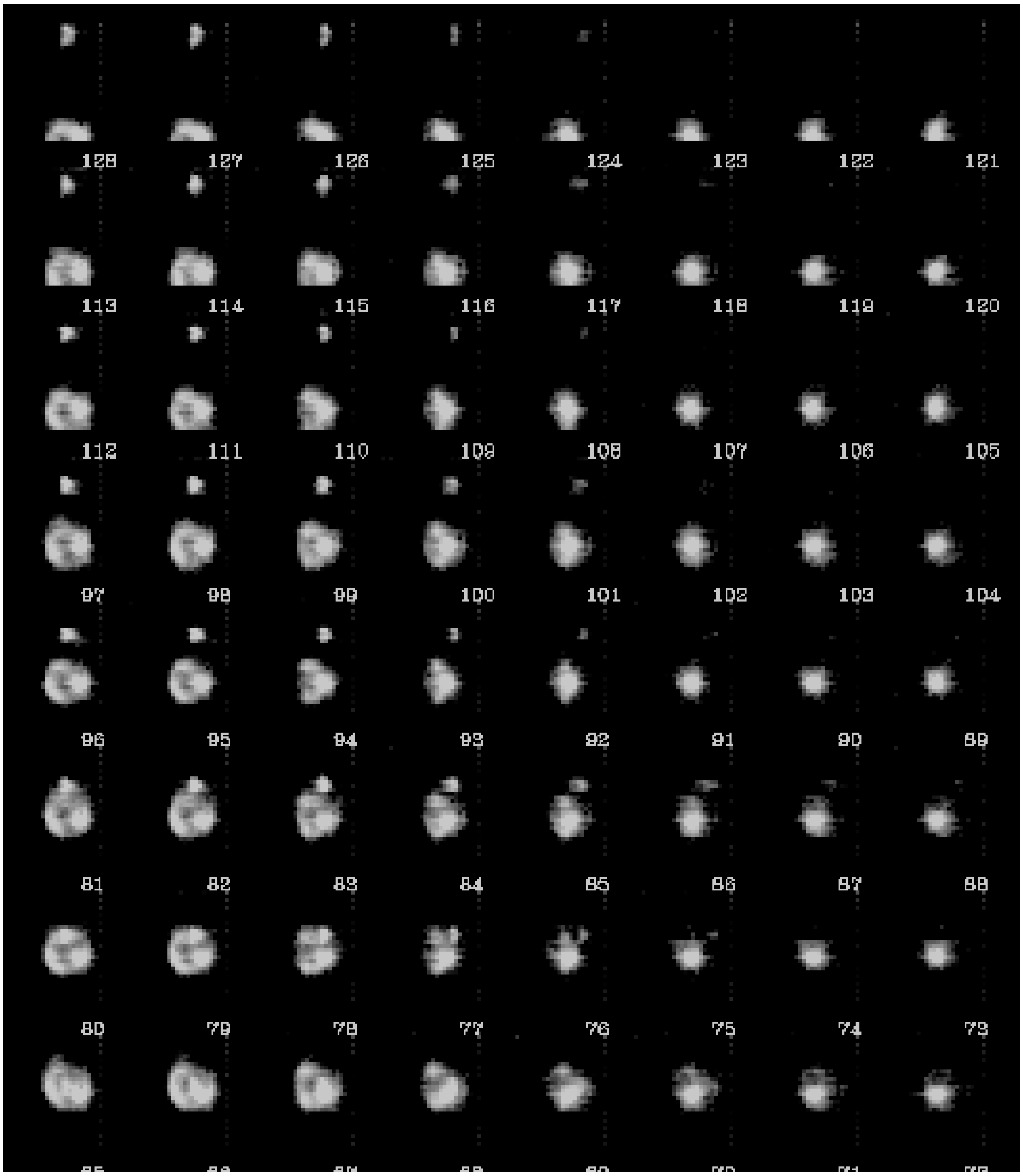

Figure 7: Discontinuous behaviour of ghosts when a point source moves around this region of the second half of a 8×16 raster (CVF at 5 μm with 6 arcsec PFOV in Rev. 740)

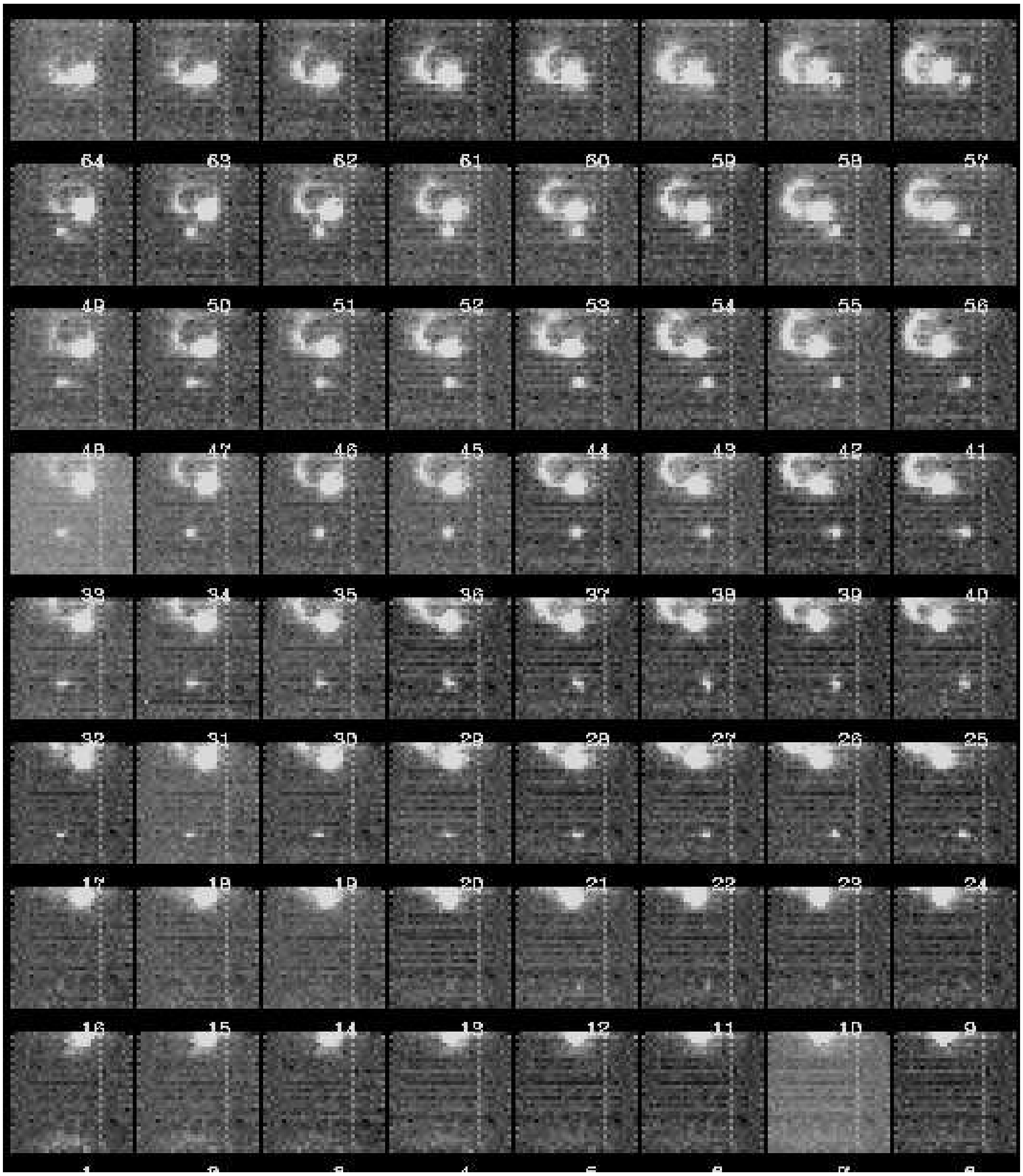

Figure 8: Discontinuous behaviour of ghosts when a point source moves around this region of the first half of a 8×16 raster (CVF at 9 μm with 6 arcsec PFOV in Rev. 740)

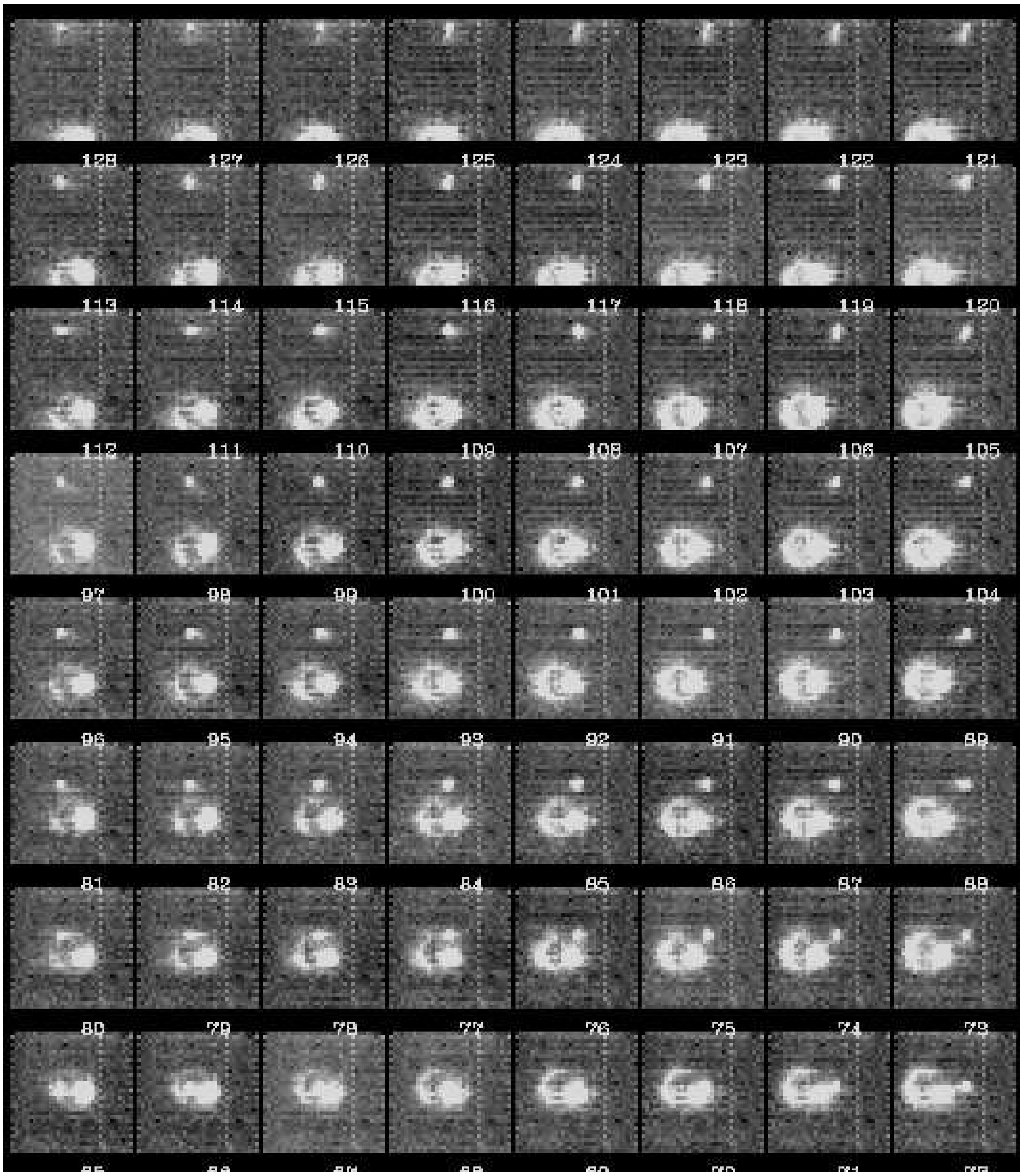

Figure 9: Discontinuous behaviour of ghosts when a point source moves around this region of the second half of a 8×16 raster (CVF at 9 μm with 6 arcsec PFOV in Rev. 740)

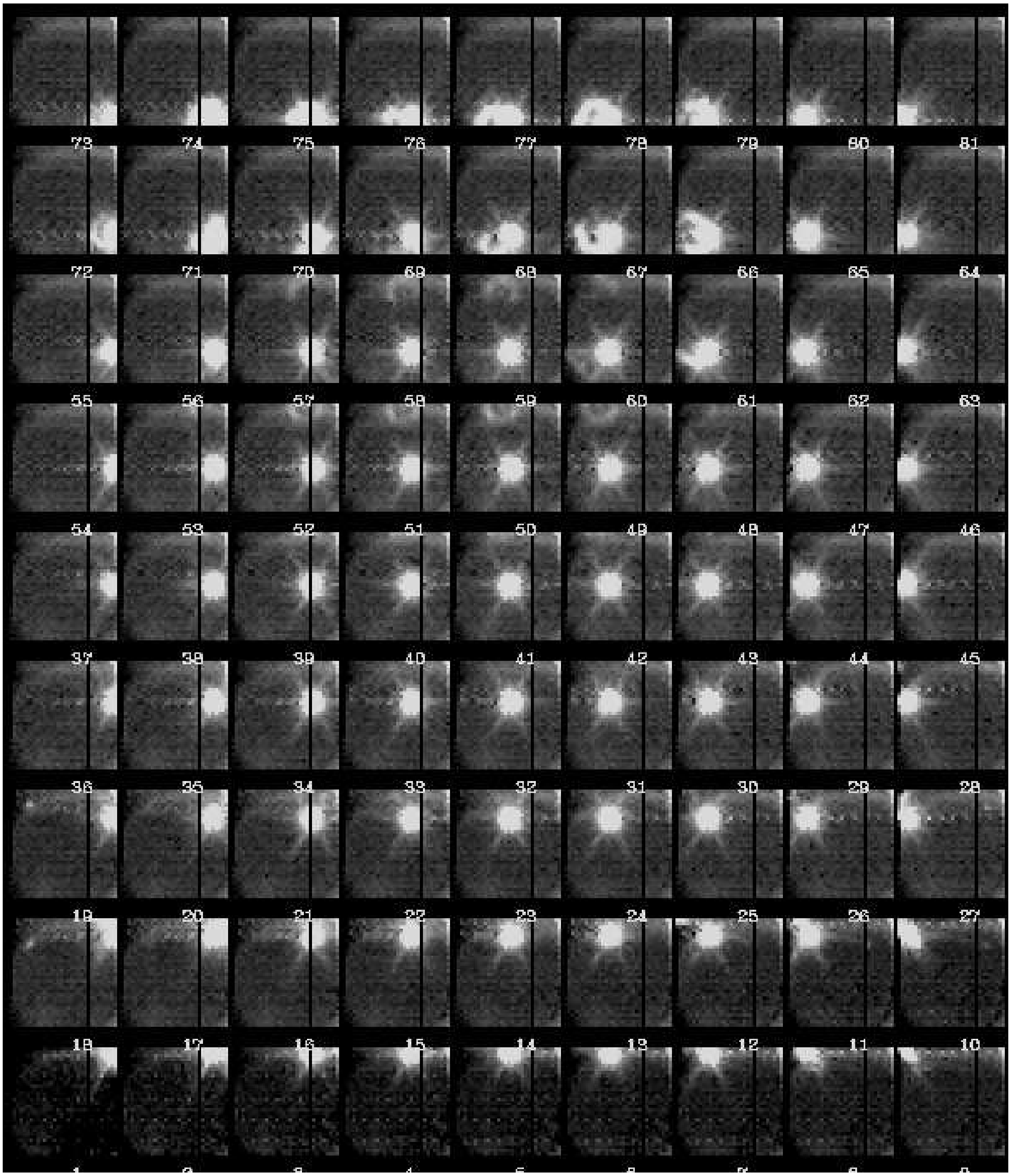

Figure 10: Global behaviour of ghosts when a point source moves over the detector (LW3 filter at 15 μm with 6 arcsec PFOV in Rev. 576)

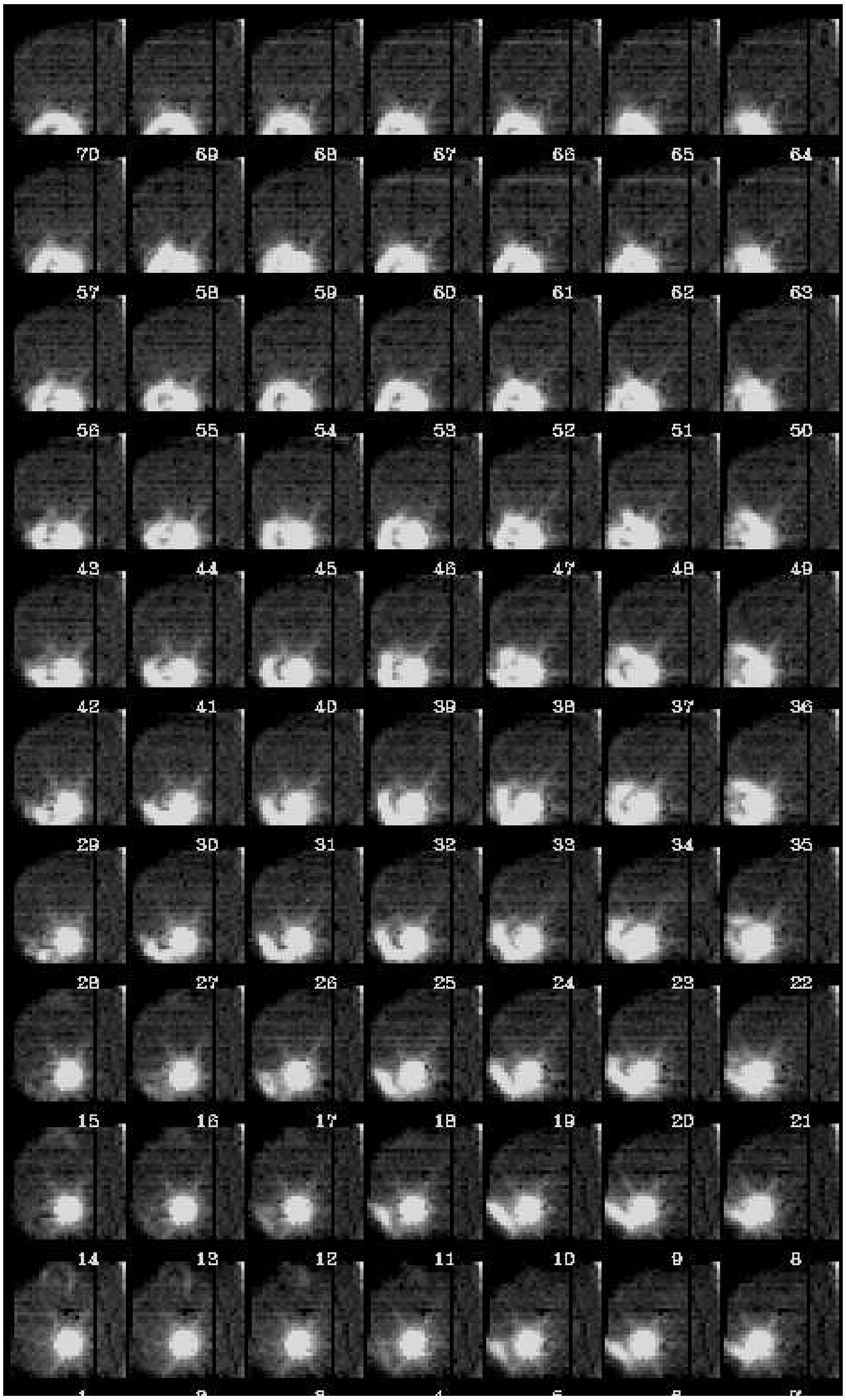

Figure 11: Discontinuous behaviour of ghosts when a point source moves around this region of a 7×10 raster (LW3 filter at 15 μm with 6 arcsec PFOV in Rev. 740)

and a diffuse excess brightness on the side of the source as seen in Fig. 2. The measured flux of this source based on the SWS calibration observations is reported (private communication) to be roughly 3000 to 5000 Jy. This means that the brightest pixel of the stray light is about 10^{-5} to 10^{-6} times fainter than the flux of the source, corresponding to the predicted values in the pre-flight optical modelling (see ISO Observer's Manual [4]).

On the contrary we call ghost an undesirable light caused by a source inside the ISOCAM field. The main ghost produced by the reflections on the detector plane and then on the filter plane is seen as an extended circular shape and its size depends on the lens used for the observation (see Fig.3).

Fig. 4 shows the typical global behaviour of ghosts observed when ISOCAM is used with a CVF and 6 arcsec PFOV lens. As the CVF surface is almost perpendicular to the optical axis in the camera, the ghost falls approximately on the point source image. One can notice a more point-like fainter ghost which falls approximately at the symmetrical position relative to the detector centre. We will call "primary ghost" the strong extended one and "secondary ghost" the faint point-like one. The numbers in the Fig. 4 are the raster point numbers. The point source image goes from the upper right corner to the lower left corner following the 9×5 raster pattern. The primary ghost shows a ring-like shape corresponding to a defocussed and distorted pupil image. It is slightly off-centered relative to the point source. The integrated flux of this ghost can reach 28% of the source flux (see also Okumura 1998 [5]). The secondary ghost is compact and moves from the lower left corner to the upper right corner exactly in the opposite way of the point source. The integrated flux of this ghost can reach 9% of the source flux (see also Biviano et al. 1997 [1] and 1998 [2]). Ghosts of still fainter flux are certainly present, but they are difficult to be identified as ghost.

Fig. 5 shows a similar observation of a 6×4 raster with a CVF at 5 μm and the 3 arcsec PFOV lens. The primary ghost has an almost fixed position regardless of the position of the point source and it has a rather well focussed pupil image showing even the central hole and the tripods structure. The secondary ghost is not easily identified with the 3 PFOV lens although a vertical bright band is noticeable in some raster points (for example No.5, 8, 18 and 19).

For some wavelengths corresponding to certain CVF positions, the ghost images show a discontinuous variation. Fig. 6 to 7 show an example of discontinuity at a CVF position corresponding to the wavelength of 5 μm. A 8×16 raster is shown divided into two figures. The same features as in Fig. 4 are seen, but both the primary and the secondary ghosts become very faint when the point source image is on the right side of the detector. Fig. 8 to 9 show another example at the wavelength of 9 μm. The discontinuity is much less clear but the ghost is fainter this time on the left side of the detector than on the right side. These wavelengths correspond to the two extreme positions of a LW CVF. The discontinuous intensity variation of the ghosts seen here is suspected to be connected to the edge of a CVF and the filter mount.

Fig. 10 shows the global behaviour of ghosts observed with a filter. As the filters have been tilted with respect to the optical axis, one might think that the ghosts are rejected outside the detector. Nevertheless, the tilt of 5° does not reject the ghosts far enough with 6 and 12 arcsec PFOV lenses. Even when the point source is at the detector centre (raster point No.41), non negligible fraction of the primary ghost is seen at the upper part of the detector. It is almost entirely seen in the raster point No.59. The primary ghost is now separated from the point source due to the tilt of the lens and behaves just like the ghost with a CVF except that it is vertically displaced by about 16 pixels. If this is true, then we should find also the secondary ghost when the point source is in the upper part of the detector. This is indeed seen especially clearly in the raster point No.19 and No.36. The integrated intensities of the ghosts are fainter than those observed with a CVF and the primary ghost reaches about 18%. In addition to this

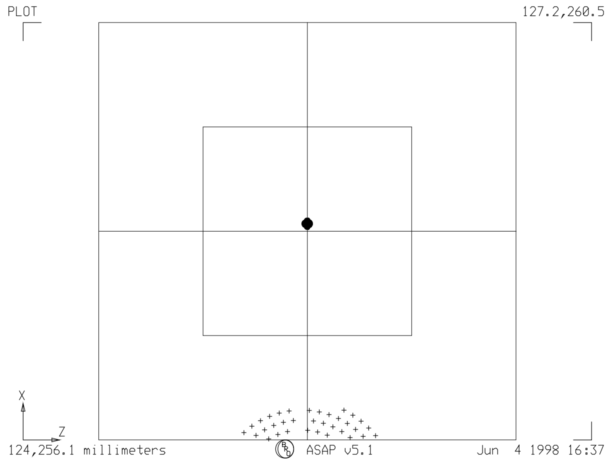

Figure 12: The primary ghost for a filter is displaced toward the positive Z-axis due to its tilt of 5°. With 6 arcsec FPOV lens a fraction of it is seen at the edge of the detector.

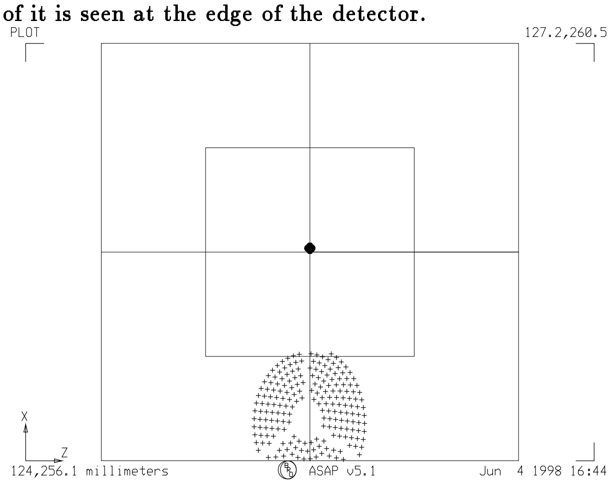

Figure 13: The primary ghost for a filter is displaced toward the positive Z-axis due to its tilt of 5°. With 12 arcsec FPOV lens a large fraction of it is seen in a elliptical form.

known behaviour, it is also seen a strange discontinuous behaviour of the ghosts. In the raster points 66 to 68 and 76 to 79 the primary ghost falls on the point source as if we are looking at an observation with a CVF. Fig. 11 shows this region in more detail. It is clearly seen that this is a discontinuous behaviour. The ring-like shape of the primary ghost is even cut horizontally and this cut is located about 10 pixels from the bottom. This CVF-like ghost is possibly due to a non tilted surface near the filter plane. The filter mount is believed to be a good candidate, which may explain also the discontinuous behaviour of the ghost.

3 Simulations of ghosts using ASAP

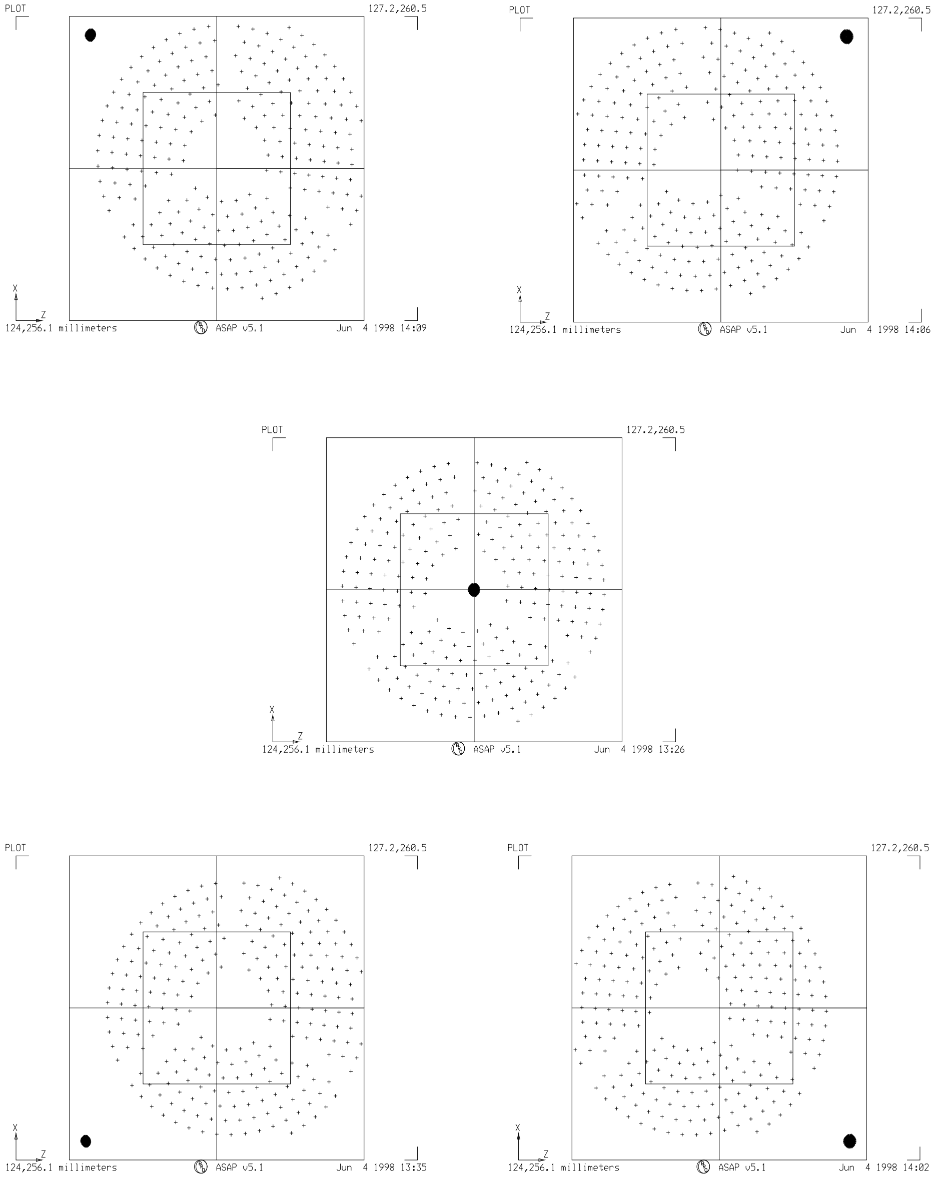

Figure 14: With a CVF and 3 arcsec FPOV lens, the primary ghost covers a large part of the detector and its location depends very little on that of the point source.

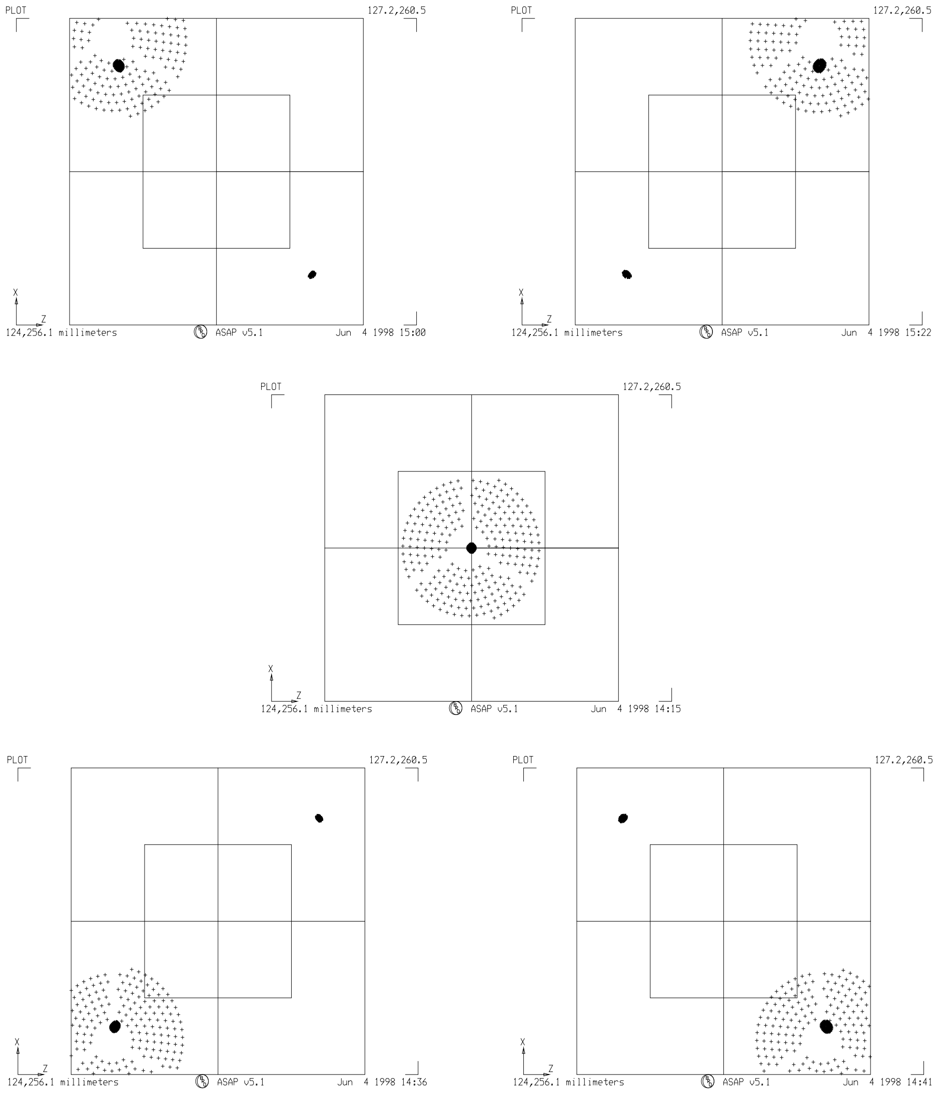

Figure 15: With a CVF and 6 arcsec FPOV lens, the primary ghost is always around the point source whereas the secondary ghost is point-like and is located near the symmetrical point of the source with respect to the detector centre.

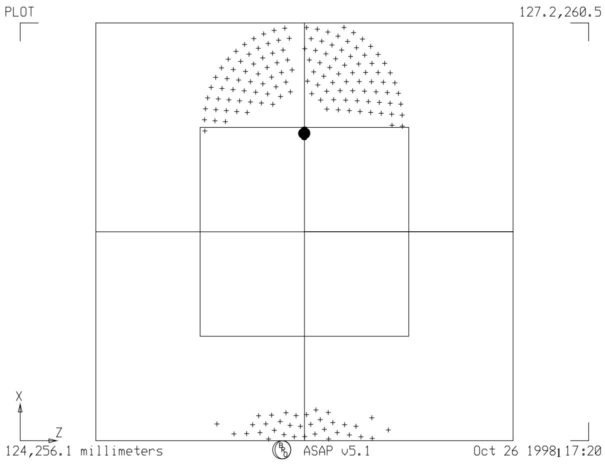

Figure 16: The discontinuous behaviour of the ghosts with a filter at 6 arcsec lens is quantitatively reproduced in the optical model.

In order to understand the origin of ghosts in the ISOCAM images, an optical model of the instrument is being elaborated using optical modeling program ASAP version 5 [1]. The model is still to be completed but some preliminary results are interesting enough to be presented here.

The main result is that the primary ghost is of the same nature for 3 and 6 arcsec PFOV as it can be suspected from the observations. It is generated by a beam reflected first on the detector plane and next on one of the filter surfaces, then it reaches the detector plane. The filter tilt of 5° gives an offset of the primary ghost (Fig. 12 for 6 arcsec POFV and Fig. 13 for 12 arcsec POFV lens). The ghost is rejected to the lower part instead of the upper part because of the axis convention. In the calibration observations data shown in the previous section, the spacecraft Y-axis points toward the right and the Z-axis toward the bottom. In the ASAP simulation results, the spacecraft Y-axis points toward the left and Z-axis toward the top. Therefore there is a rotation of 180° between them.

The secondary ghost is generated after a second back and forth flight of the beam between the detector and the filter. As observed it shows up symmetric to the point source relative to the optical axis. Fig. 15 shows this behaviour for the 6 arcsec PFOV lens. When using the 3 arcsec PFOV lens, the secondary ghost is not focussed on the detector plane, hence is not detectable as appears on Fig. 14.

It is important to note that the spot diagrams shown here does not represent the brightness distributions but the intersections of rays with the detector plane and each of these rays may have a different intensity. Nevertheless, these diagrams contain only sets of rays which form the point source image and the ghost(s). Therefore, they can be considered as giving a reliable indication of the ghost location and extent, but not of the brightness distribution within the ghost.

Fig. 16 shows the discontinuous behaviour observed in Fig. 11. As mentioned before, this discontinuity is due to the reflection on a tilted filter and on its non-tilted mount.

Fig. 17 shows the measured and modeled optical response to a uniform brightness distribution (optical flat-fields) for a set of CVF wavelengths. The two lobes structure is qualitatively reproduced by the optical model (see also Biviano et al. [2]).

Fig. 18 shows the measured and modeled optical flat-fields for a set of filters. The optical

[1]ASAP is a package of BRO. Our work is carried out under the licence given to Institut d'Astrophysique Spatiale at Orsay (IAS)

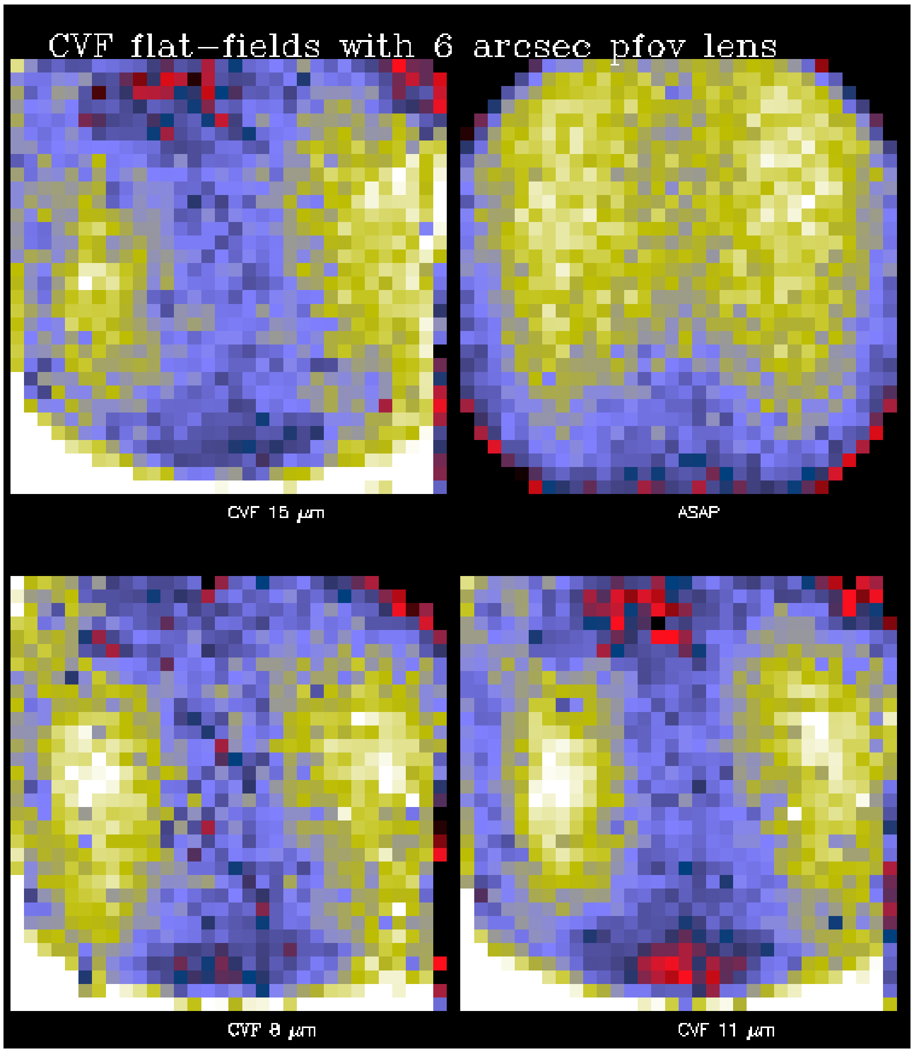

Figure 17: Comparison between measured and modeled optical flat-field for a CVF.

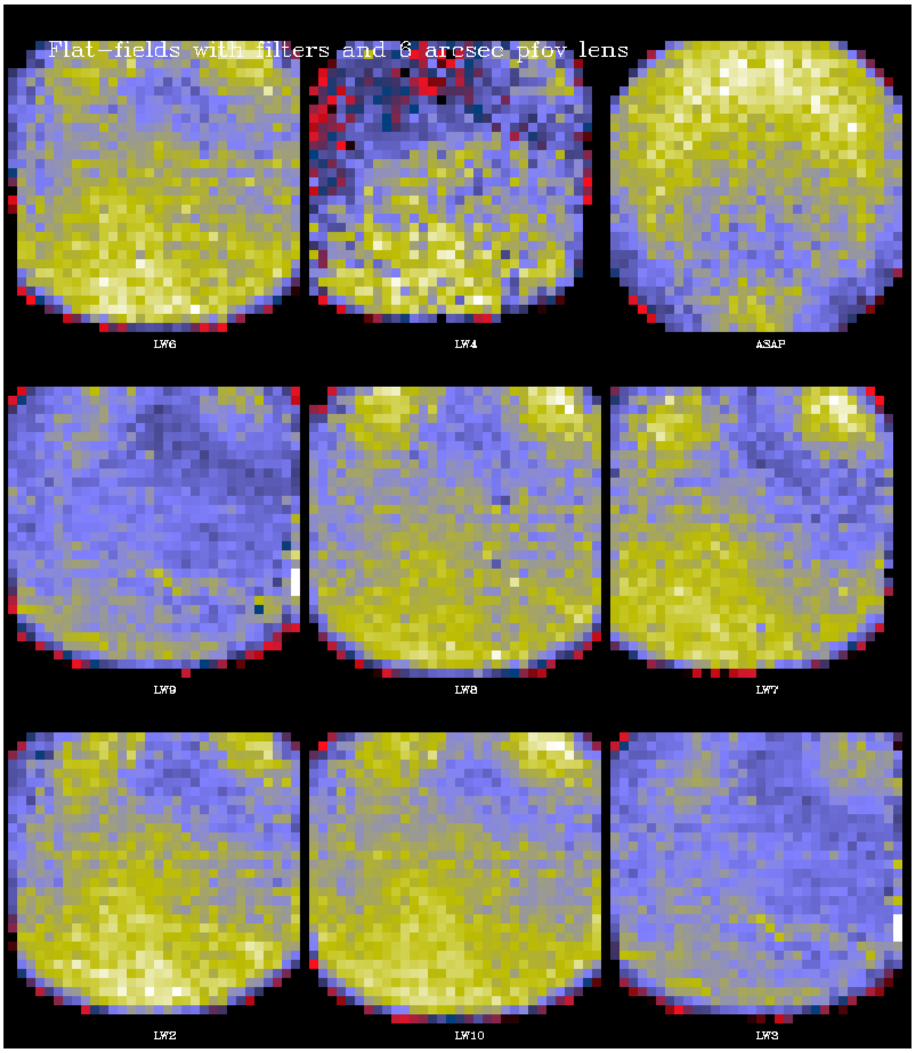

Figure 18: Comparison between measured and modeled optical flat-field for filters.

model produces an irregular illumination due to the ghosts. This pattern seems to have an vertical offset with respect to those observed in the measured flat-fields, indicating that further adjustments of optical parameters are still needed to the model.

For an extended source required for a optical flat-field, the number of rays in the optical model should be large enough to reach a reasonable signal to noise ratio. For the pattern seen in ISOCAM's optical flat-fields, it is required to generate at least 2 millions of rays to overcome the sampling noise. This requires 2 to 3 days of CPU time on a HP computer we use.

4 Preliminary conclusion

The brightest (primary) ghost image is found to be a defocussed pupil image formed by the beam of the point source reflected on the detector plane and then on the filter plane to reach the detector again. The secondary ghost image well observed with 6 arcsec PFOV lens is found to be caused by the same beam as the primary ghost but the same reflections are repeated twice to reach eventually on the detector. The results of the optical simulation presented here are still preliminary and there still remains much to be worked out. Our optical model can not yet reproduce every features observed in the dedicated observations. Further development must be focussed on more quantitative results comparable to the observations. For example deeper studies of the following points are needed:

(1) Relative intensities of the primary and secondary ghosts with respect to that of the point source

(2) Flat field pattern with a CVF and with a filter

(3) Wavelength dependence of the intensity of the ghosts with the CVFs (Biviano [3])

(4) Discontinuous feature of the ghosts

(5) Non-uniform brightness of the pupil image in the primary ghost

In order to reproduce (1) the transmission and reflection coefficients of the detector surface and the filters should be set correctly for a set of wavelengths. The same parameters for each segment of the CVFs are needed for (2) and (3). A good knowledge of the optical parameters of the filter mounts are needed for (4). And we have to search for the reason among some possibilities for (5).

The optical model will be used in a first phase to flag the expected ghosts of bright sources, mainly in CVF observations. An interpolation scheme for the calibration data will be studied, and correction possibilities will be investigated.

Acknowledgements

We are grateful to François Sibille who gave us useful information on the parameters of the optical elements and his knowledge on the ISOCAM instrument through its conception phase.

References

[1] A. Biviano, B. Altieri., J. Blommaert, F. Boulanger, D. Cesarsky, K. Okumura, W. Reach Topics in ISOCAM Spectroscopy Calibration. Proceedings first ISO workshop on analytical spectroscopy, 1997.

[2] A. Biviano et al. The ISOCAM cvf calibration report 1998.

[3] A. Biviano et al. The ISOCAM calibration error budget report 1998.

[4] ISO Observer's Manual. ESA, 1994.

[5] K. Okumura. ISOCAM PSF report. 1998.

[6] M. Pérault et al. Infrared Space Observatory camera calibration facility and preflight characterization 1994, Optical Engineering 33, 762, Provided by the NASA Astrophysics Data System